Supporting Information

Facile Synthesis of Nickel-Iron/Nanocarbon Hybrids as Advanced Electrocatalysts for Efficient Water Splitting

Xing Zhang, Haomin Xu, Xiaoxiao Li, Yanyan Li, Tingbin Yang, Yongye Liang*

Department of Materials Science and Engineering, South University of Science and Technology of China, Shenzhen, 518055, China

*To whom correspondence should be addressed. E-mail: Liangyy@sustc.edu.cn

Additional Experimental Section

Post-deposition of metallic $Ni_{0.9}Fe_{0.1}$ nanoparticles on commercially multi-walled CNTs was referred to the reported work with slightly modification.[1, 2] The synthetic procedures mainly included three steps:

1) **Synthesis of mildly oxidized CNTs (mo-CNTs).**

Multi-walled CNT (FloTube 9000 from CNano Technology Ltd.) was first purified by calcinations at 500 ℃ for 1 h and washing with dilute hydrochloric acid (10%). The purified CNT (1 g) was oxidized by reacting with 1 g of $KMnO_4$ based on the reported procedure.[1]

2) **Synthesis of Ni-Fe hydroxide on mo-CNTs.**

For the synthesis of Ni-Fe hydroxide on mo-CNTs (Ni-Fe$(OH)_x$/mo-CNTs), 10 mg oxidized mo-CNTs were sonicated in 20 ml of anhydrous N,N-dimethylformamide (DMF) for 10 min, followed by the addition of 1.17 ml of 0.2 M $Ni(OAc)_2$ and 0.13 ml of 0.2 M $Fe(NO_3)_3$ aqueous solution. The mixture was vigorously stirred at 90℃ in an oil bath for 4 h. Afterwards, the suspension was centrifuged and washed with H_2O twice to get rid of DMF. The resuspended solution was lyophilized to get solid Ni-Fe$(OH)_x$/mo-CNTs hybrid.

3) **Synthesis of $Ni_{0.9}Fe_{0.1}$-CNTs.**

The solid Ni-Fe$(OH)_x$/mo-CNTs were then annealed in a tube furnace at 500 ℃ and constant pressure of 1.5 torr under Ar atmosphere (100 sccm) for 2 h. The furnace was constantly pumped to get rid of the H_2O and O_2 generated during the reaction and maintain low pressure in the furnace. After that, the furnace was slowly cooled down to room temperature naturally and the solid products were taken out and ready for use.

Supplementary Figures

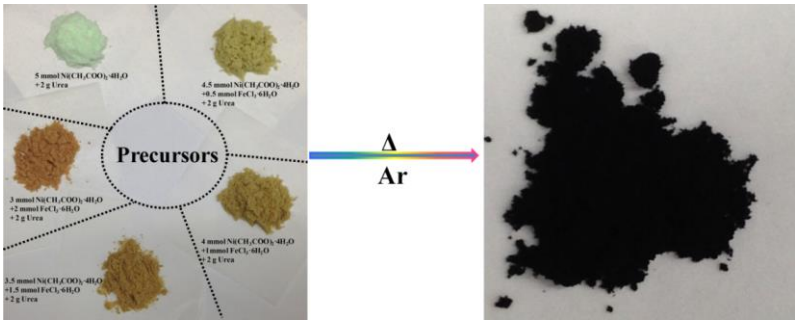

Figure S1. Digital images of the precursors (left panel) and products (right panel) after pyrolyzing under Ar atmosphere.

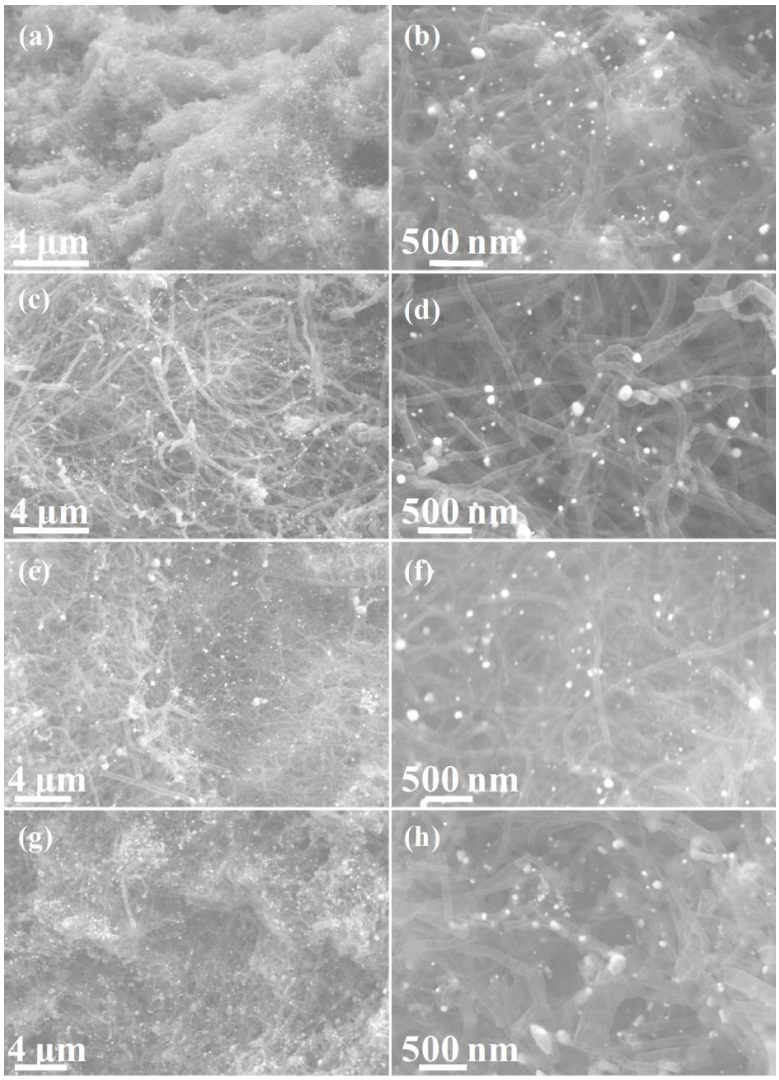

Figure S2. SEM images of Ni/NC (a) and (b), $Ni_{0.8}Fe_{0.2}$/NC (c) and (d), $Ni_{0.7}Fe_{0.3}$/NC (e) and (f), $Ni_{0.6}Fe_{0.4}$/NC (g) and (h).

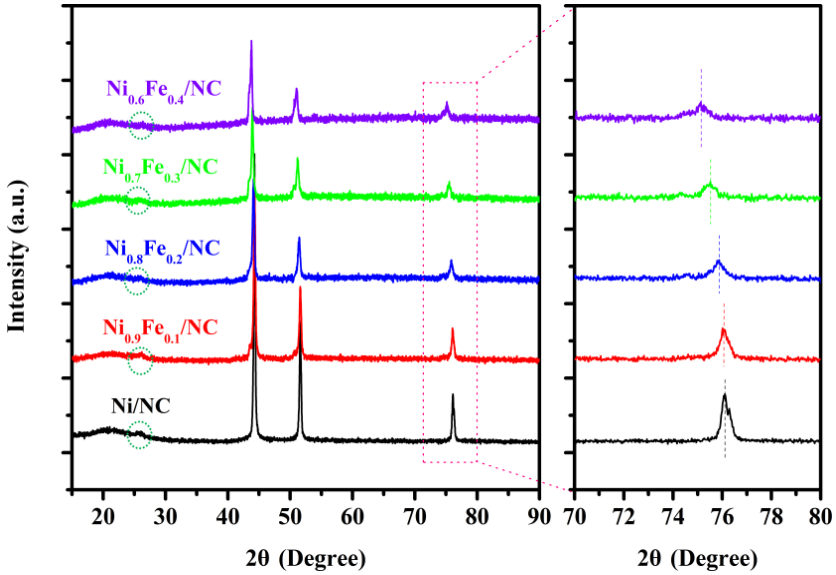

Figure S3. XRD patterns of Ni/NC, $Ni_{0.9}Fe_{0.1}$/NC, $Ni_{0.8}Fe_{0.2}$/NC, $Ni_{0.7}Fe_{0.3}$/NC, $Ni_{0.6}Fe_{0.4}$/NC. The right panel shows the magnified XRD peaks as indicated by the pink rectangular dotted frame to show the negative shift of 2θ angles with increasing doping concentrations of Fe. It's implied that the lattice constants are shifted to higher values, which indicates the substitutional incorporation of Fe ions into the nickel cubic structure.

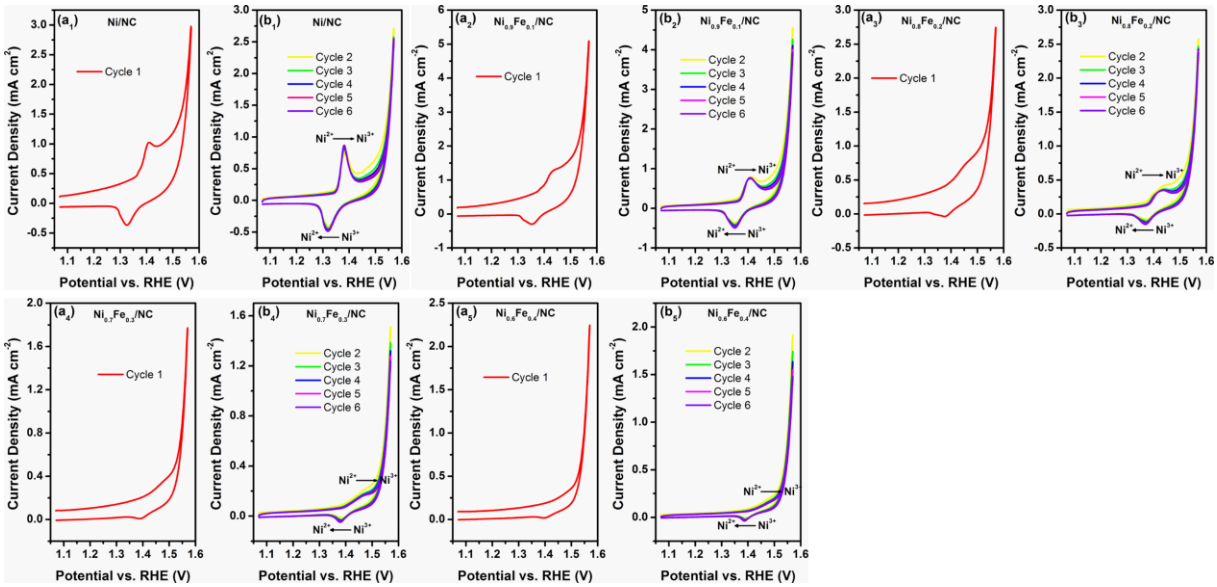

Figure S4. First six CV curves of the $Ni_{1-x}Fe_x$/NC samples on GCE collected before the OER electrochemical characterizations.

For all the samples, the first CV cycle exhibited a significantly larger integrate current in the anode scan than the cathode scan before the onset of OER, indicating an oxidation

reaction occurred on the metallic species in $Ni_{1-x}Fe_x$/NC in this potential region. In the following five CV cycles, the CV curves became to trace the previous CV curves and exhibited a reversible $Ni^{2+} \rightarrow Ni^{3+}$ redox peaks. It can be found that the position of this redox peak shifted to higher potential region with higher Fe incorporation content in $Ni_{1-x}Fe_x$/NC.

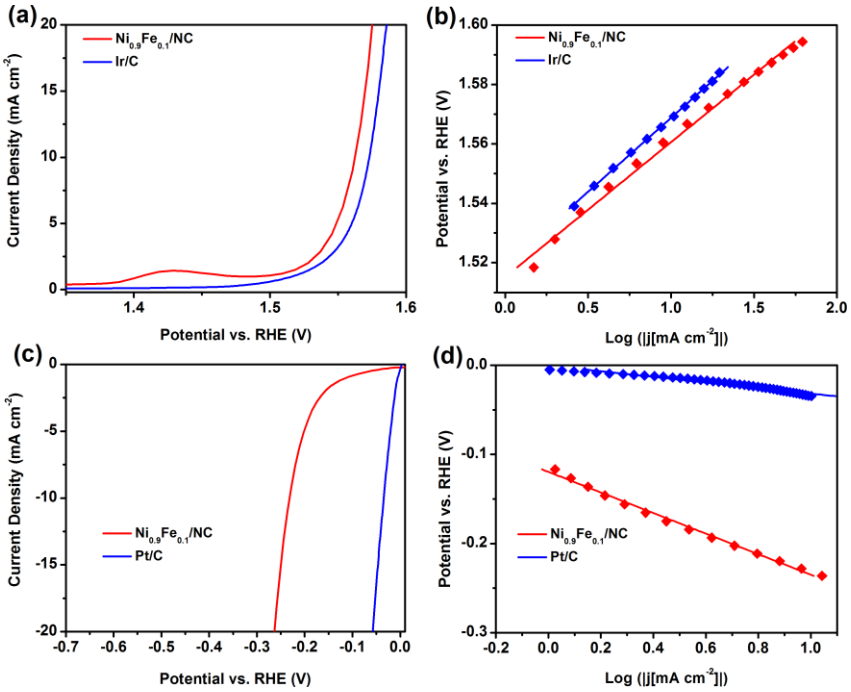

Figure S5. (a) LSV curves and (b) Tafel plots of $Ni_{0.9}Fe_{0.1}$/NC and Pt/C in HER potential window. (c) LSV curves and (d) Tafel plots of $Ni_{0.9}Fe_{0.1}$/NC and Ir/C in OER potential window.

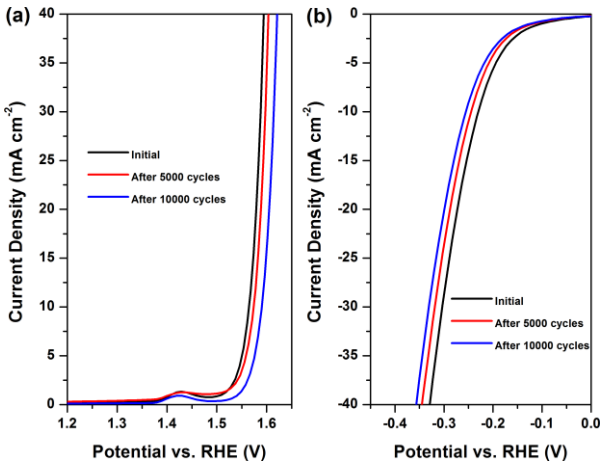

Figure S6. Accelerated durability tests by cycling the catalysts ($Ni_{0.9}Fe_{0.1}$/NC on GC electrode) at scan rate of 50 mV/s in the range between 1.2 and 1.6 V vs. RHE for OER (a)

and between -0.4 and 0.1 V vs. RHE for HER (b). The polarization curves are recorded after every 5000 cycles under quasi-equilibrium conditions with a scan rate of 10 mV/s. After 10000 cycles, there was an increase of about 25 mV of the overpotential for achieving an OER current density of 10 mA cm^{-2}. While for HER, there was also an increase of nearly 23 mV after for achieving a HER current density of -10 mA cm^{-2} after 10000 cycles. Beside the catalyst decay, the detachment of catalysts on the surface of the glass carbon electrode during the duribility test might also account for the minor increase of the overpotentials.

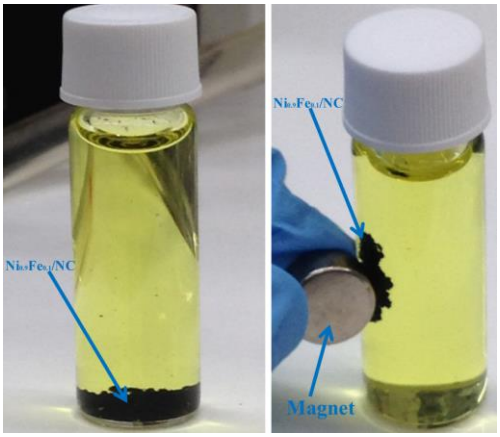

Figure S7. The digital images of $Ni_{0.9}Fe_{0.1}$/NC recorded after acid leaching in 30 wt% HCl solution for over one week. From these images we can see that the exposed metallic species in $Ni_{0.9}Fe_{0.1}$/NC were dissolved into the solution which exhibited a flavovirens color after acid leaching. However, the leached sample still exhibited strong magnetism, suggesting many metallic nanoparticles still existed in the hybrid after acid leaching.

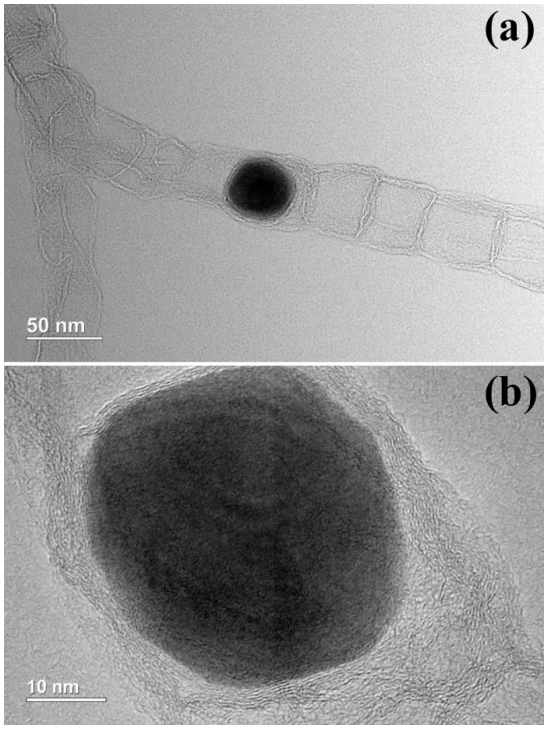

Figure S8. (a) TEM and (b) HRTEM images of $Ni_{0.9}Fe_{0.1}$/NC sample after acid leaching. These results indicated that the metal nanoparticles were completely encapsulated in the CNTs which could not be removed by acid leaching.

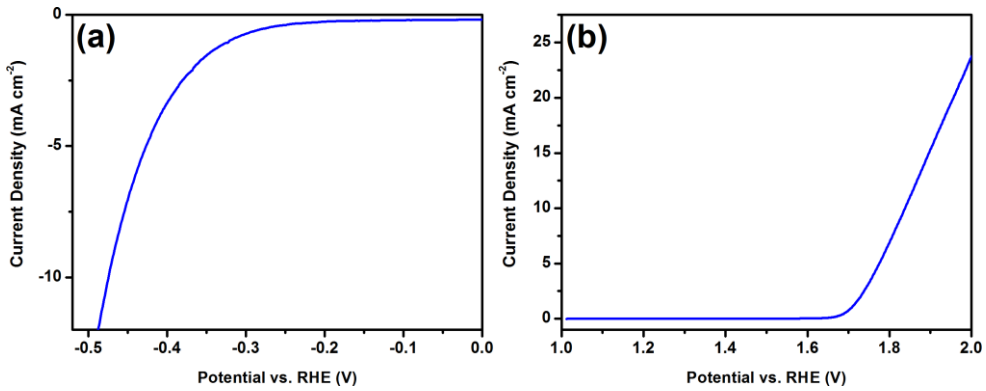

Figure S9. LSV polarization curves for (a) HER and (b) OER of $Ni_{0.9}Fe_{0.1}$/NC sample after acid leaching.

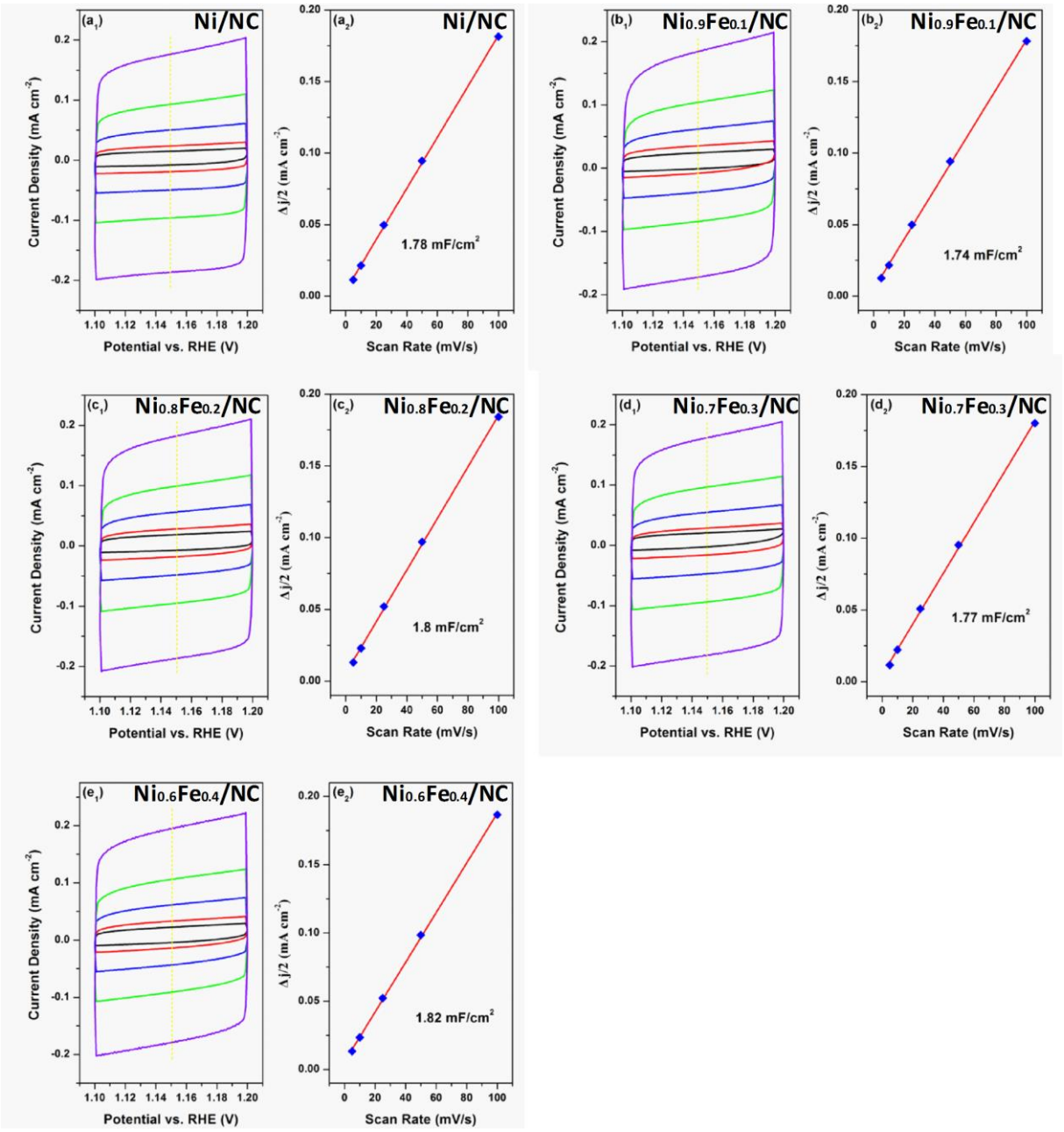

Figure S10. (a_1), (b_1), (c_1), (d_1) and (e_1) Cyclic voltammograms curves of the $Ni_{1-x}Fe_x$/NC sample (0.2 mg cm^{-2} on GC electrode) measured in a non-Faradaic region at the following scan rate: 5 mV/s (purple line), 10 mV/s (green line), 25 mV/s (blue line), 50 mV/s (red line), 100 mV/s (black line); (a_2), (b_2), (c_2), (d_2) and (e_2) The plots of ($\Delta J/2$) (1.15 V vs. RHE) with different scan rate. The double layer capacitance (C_{dl}) was then estimated from the slope of the fitted the linear region.

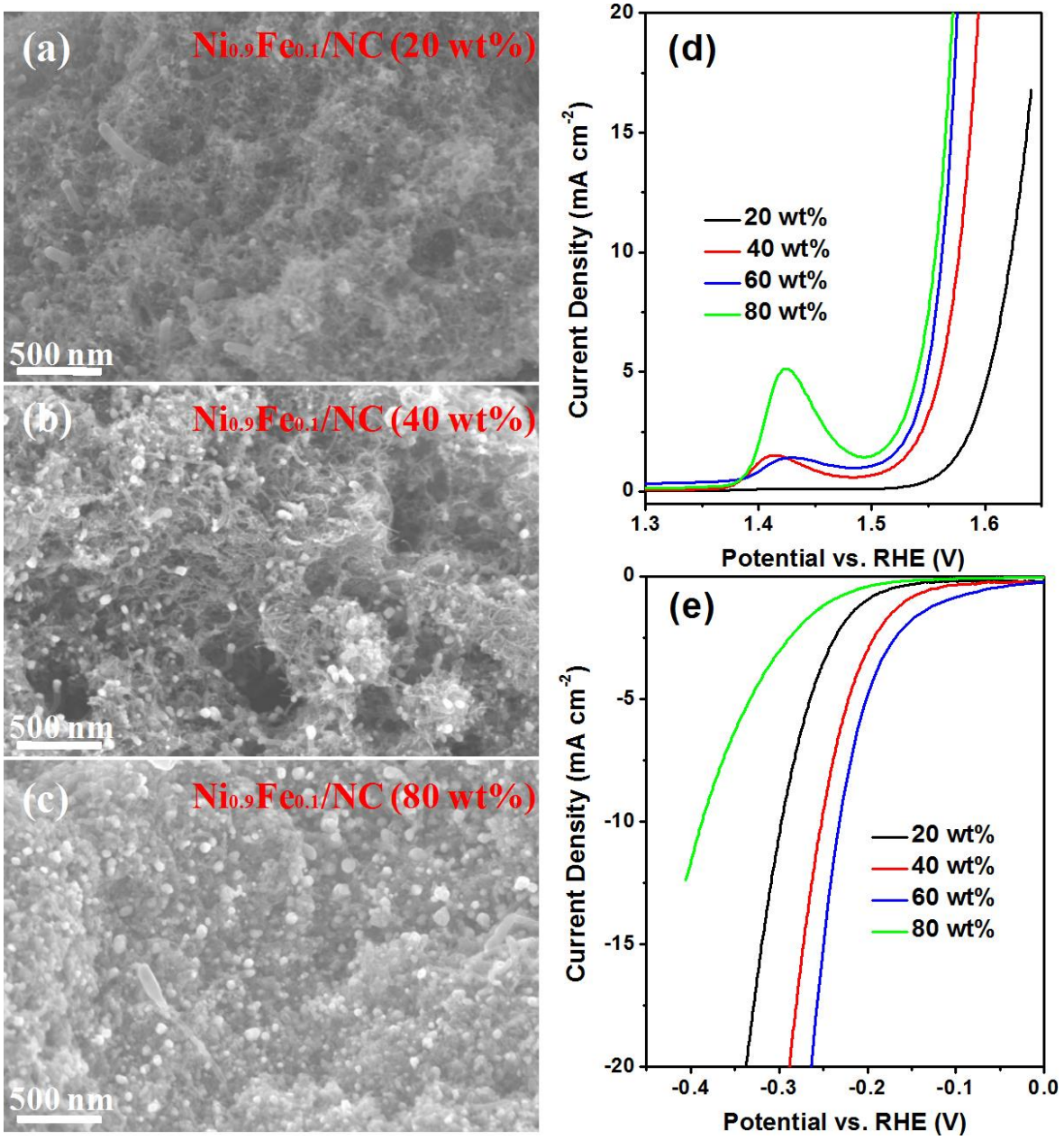

Figure S11. SEM images of $Ni_{0.9}Fe_{0.1}$/NC with metal content of (a) 20 wt%, (b) 40 wt% and (c) 80 wt %; (d) and (e) Summaries of the LSV curves of $Ni_{0.9}Fe_{0.1}$/NC with metal content of 20 wt%, 40 wt%, 60 wt% and 80 wt % for (d) OER and (e) HER.

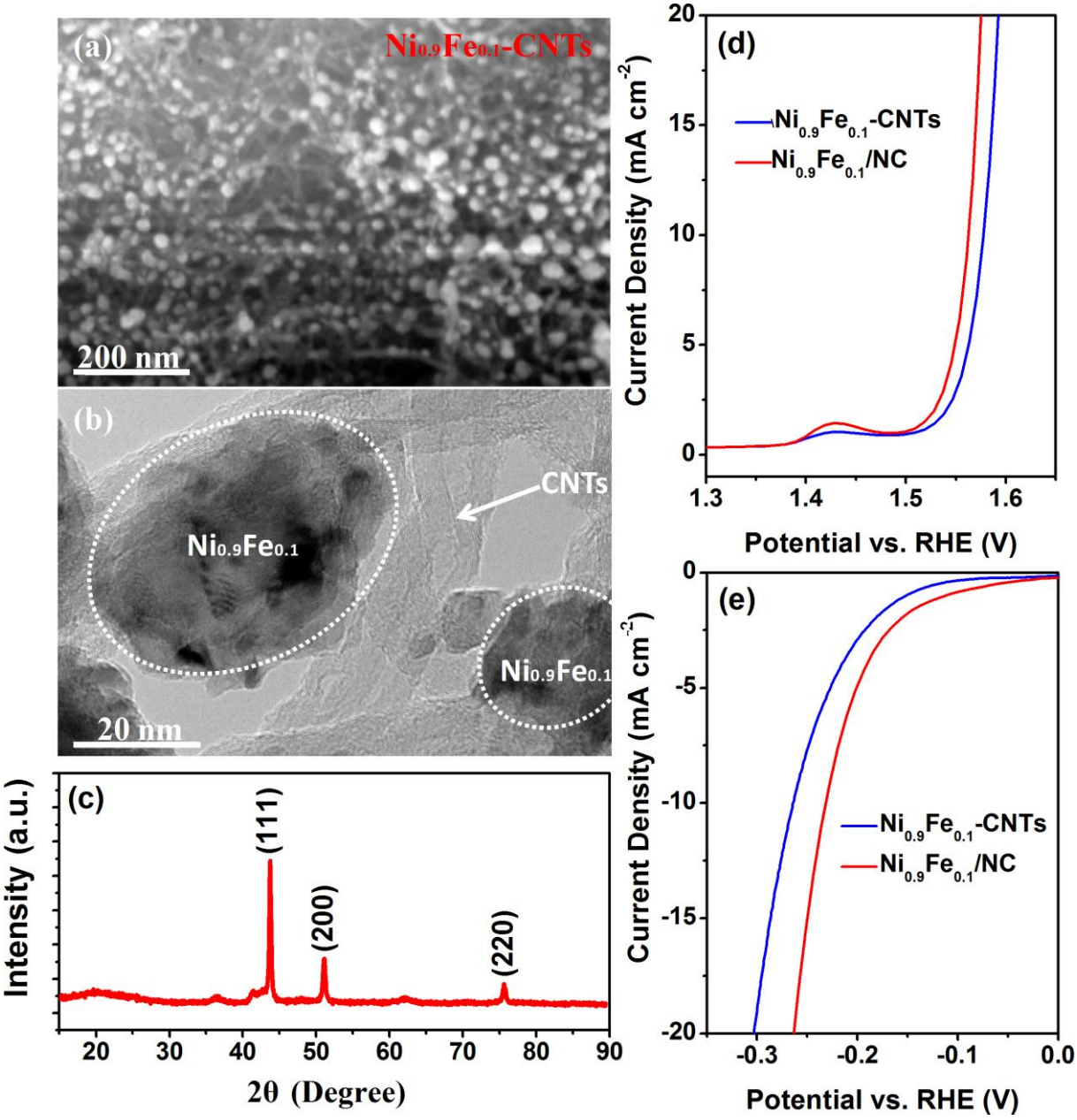

Figure S12. (a) SEM and (b) TEM images of $Ni_{0.9}Fe_{0.1}$-CNTs, respectively. (c) The XRD patterns of $Ni_{0.9}Fe_{0.1}$-CNTs. It exhibits three obvious peaks which could be indexed to face-centered cubic nickel phase (JCPDS card No. 89-7128). LSV curves of $Ni_{0.9}Fe_{0.1}$-CNTs and $Ni_{0.9}Fe_{0.1}$/NC in (d) OER and (e) HER potential window, respectively.

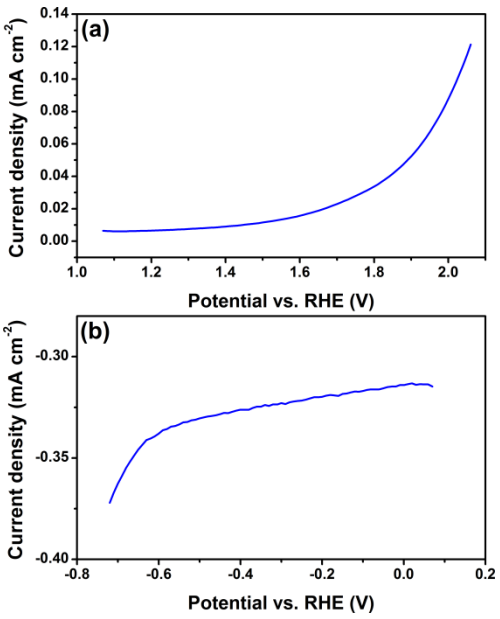

Figure S13. The LSV polarization curves of cleaning CFPs in the OER (a) and HER (b) region, respectively.

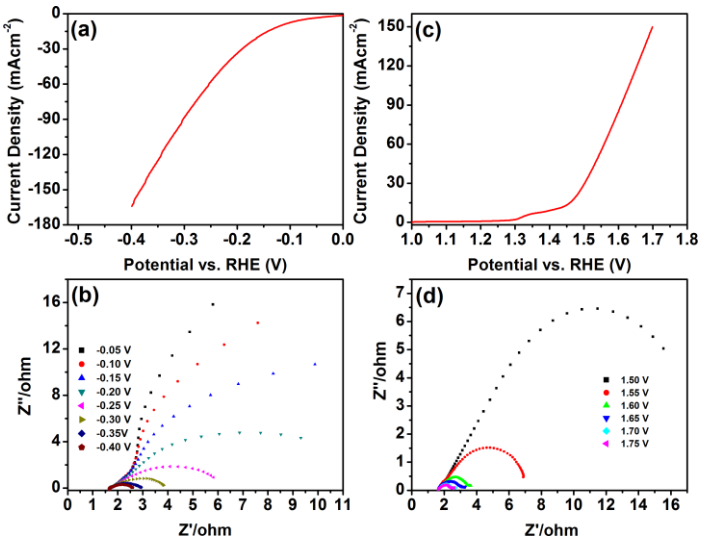

Figure S14. Polarization data of $Ni_{0.9}Fe_{0.1}$/NC on CFPs (loading: 2 mg cm^{-2}) for HER (a) and OER (c). (b) and (d) show the Nyquist plots of the EIS analysis collected at different applied potential (vs. RHE) in the proceeding region of HER and OER, respectively. The series resistance was determined to be about 1.6 Ω, which primarily comes from wiring (e.g. cables, alligator clips) and the electrolyte, while the resistance of electrocatalyst is negligible, indicating an excellent electron transport in the electrocatalyst which was endowed by the high electro-conductivity of the bamboo-like N-doped carbon nanobubes.

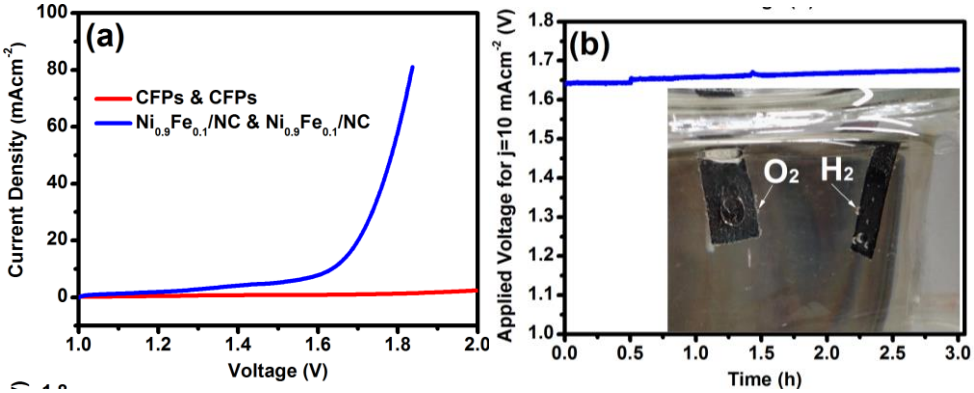

Figure S15. Bifunctional $Ni_{0.9}Fe_{0.1}$/NC loaded on CFPs for the symmetric two-electrode water splitting cell in 1 M KOH alkaline solution. (a) LSV polarization curves of $Ni_{0.9}Fe_{0.1}$/NC-CFPs electrodes and the blank CFPs electrodes. (b) Chronopotentiometric curve of the $Ni_{0.9}Fe_{0.1}$/NC-CFPs electrodes water splitting cell with a constant current density of 10 mA cm^{-2}. The digital photograph in the inset shows the hydrogen and oxygen evolution of the symmetric two-electrode water splitting cell during operation.

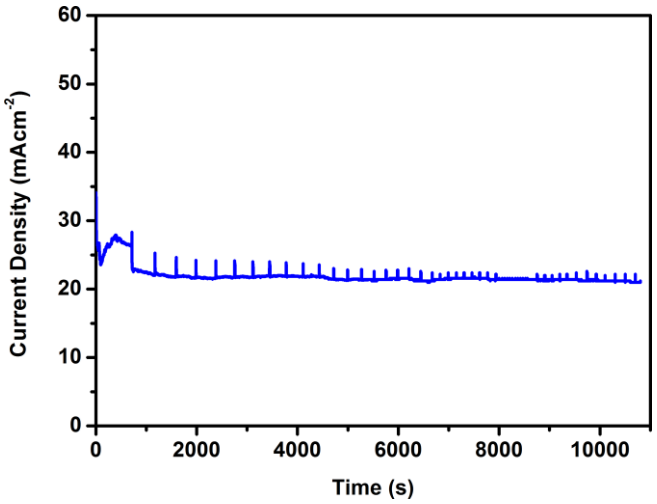

Figure S16. Chronoamperometric i-t curve for the symmetric two-electrode water splitting cell comprised of $Ni_{0.9}Fe_{0.1}$/NC on CFPs (loading: 2 mg cm^{-2}) both as the cathode and anode at an overall applied potential of 1.7 V. The spikes in the curve were attributed to the alternate processes of bubble accumulation and release on the surface of the electrodes.

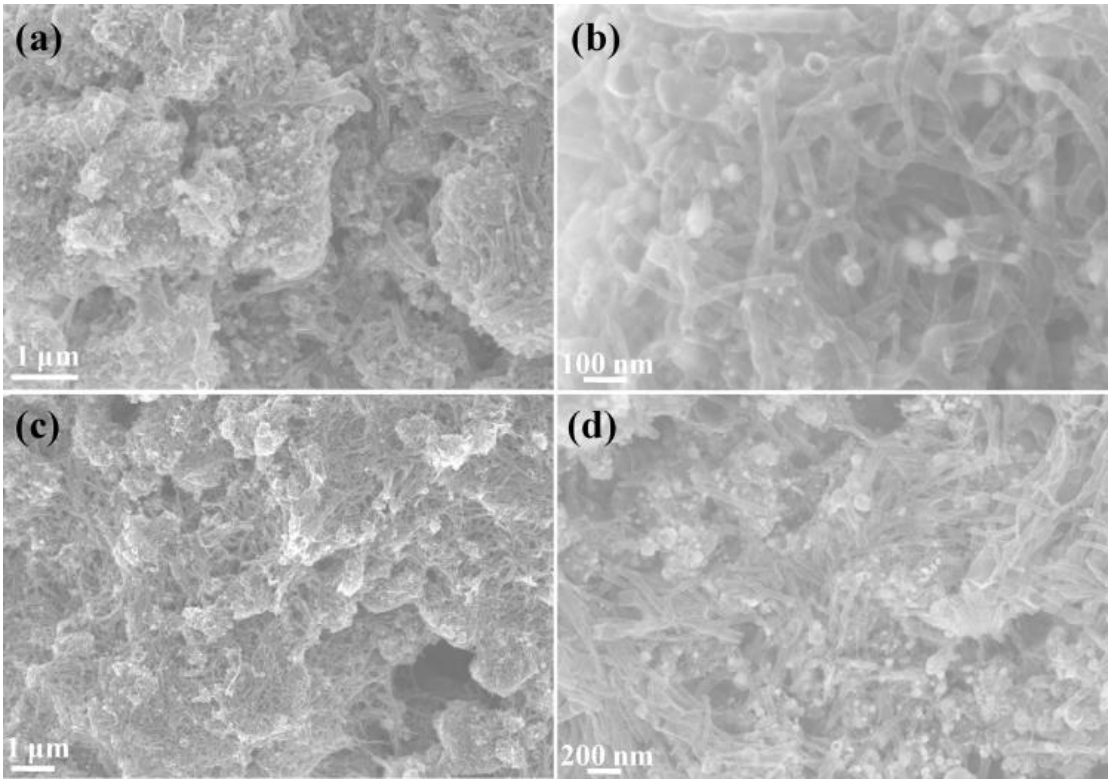

Figure S17. SEM images of $Ni_{0.9}Fe_{0.1}$/NC mixed with Nafion binder on CFPs after stability tests for HER (a,b), and OER (c, d).

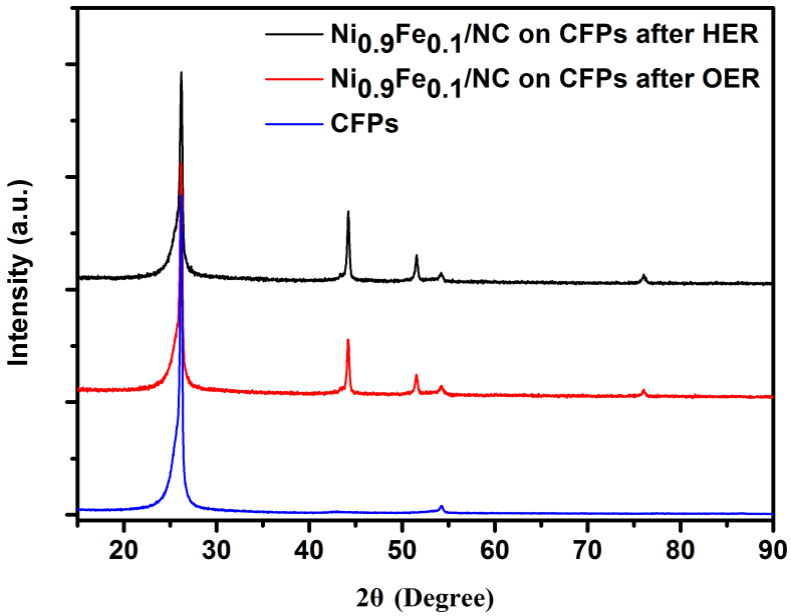

Figure S18. XRD patterns of $Ni_{0.9}Fe_{0.1}$/NC on CFPs after stability tests for HER and OER.

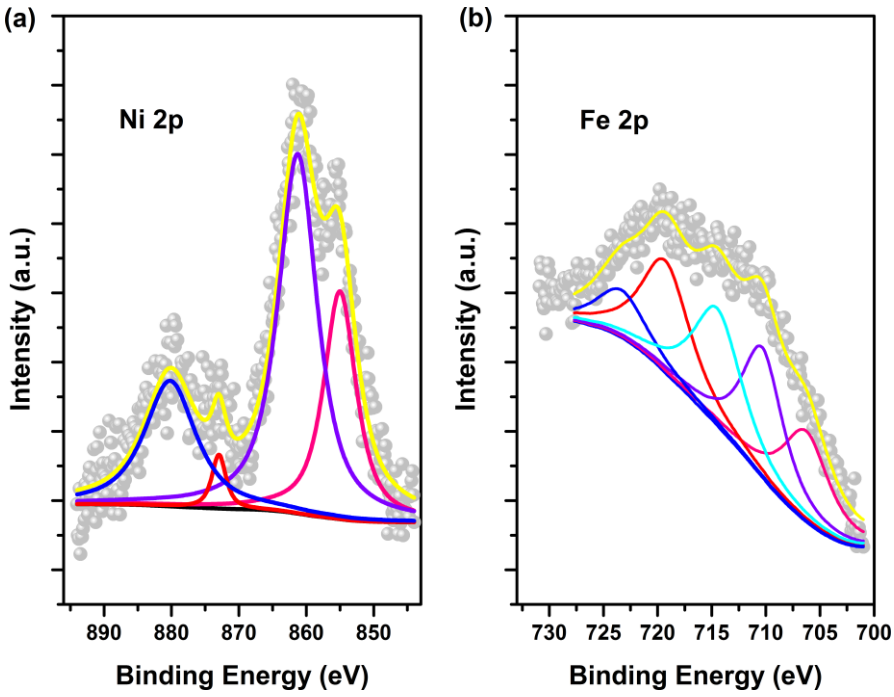

Figure S19. High-resolution XPS spectra of (a) Ni_{2p} and (b) Fe_{2p} of $Ni_{0.9}Fe_{0.1}$/NC after stability test for OER.

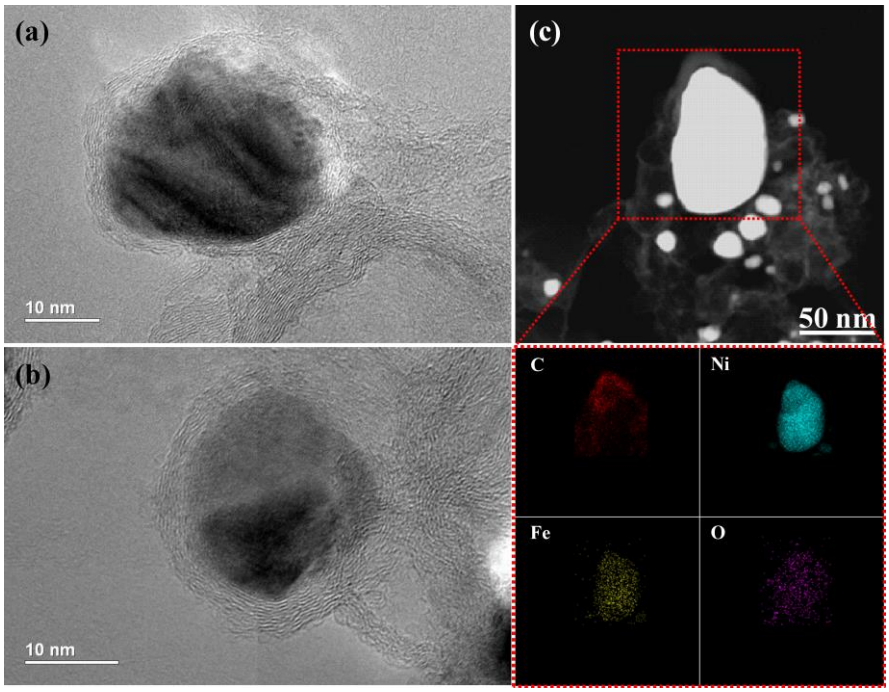

Figure S20. (a) and (b) are the High-resolution TEM images of the same sample. (c) HAADF-TEM image and the corresponding EDS mappings of the sample in the region marked with the red dotted rectangular frame.

Supplementary Tables

Table S1. Summaries of the performance parameters including Tafel slope, exchange current density and overpotential (η) for a current density of 10 mA cm^{-2} of $Ni_{1-x}Fe_x$/NC, benchmark Ir/C and Pt/C in electrocatalytic HER and OER determined from Figure 3 and Figure S5.

Tafel Analysis for OER						
Catalyst	Ni/NC	$Ni_{0.9}Fe_{0.1}$/NC	$Ni_{0.8}Fe_{0.8}$/NC	$Ni_{0.7}Fe_{0.3}$/NC	$Ni_{0.6}Fe_{0.4}$/NC	Ir/C
Tafel slope (mV/dec)	54	45	46	54	56	50
Exchange Current Density (mA/cm^{-2})	1.2×10^{-6}	5.3×10^{-7}	2.8×10^{-7}	3.0×10^{-6}	1.79×10^{-6}	1.58×10^{-6}
η (mV) for j=10 mA cm^{-2}	371	330	348	355	378	343
Tafel Analysis for HER						
Catalyst	Ni/NC	$Ni_{0.9}Fe_{0.1}$/NC	$Ni_{0.8}Fe_{0.8}$/NC	$Ni_{0.7}Fe_{0.3}$/NC	$Ni_{0.6}Fe_{0.4}$/NC	Pt/C
Tafel Slope (mV/dec)	101	111	110	119	110	31
Exchange Current Density (mA/cm^{-2})	0.073	0.092	0.03	0.024	0.007	0.972
η (mV) for j=-10 mA cm^{-2}	219	231	253	297	337	35

Table S2. Comparison of our $Ni_{0.9}Fe_{0.1}$/NC catalyst with some recently reported nonprecious OER electrocatalysts in alkaline media measured on **glassy carbon electrode**.

Catalyst	Mass loading	Overpotential vs. RHE for j=10 mA cm^{-2}	Tafel slope mV/dec	Reference
$Ni_{0.9}Fe_{0.1}$/NC	0.2 mg cm^{-2}	330 mV	45	*This work.*
Ni/N/C	0.4 mg cm^{-2}	390 mV	N/A	***Adv. Energy Mater.,*** 2015, 5, DOI:10.1002/aenm.201401660
$Mn_{0.1}Ni_1$	0.28mg cm^{-2}	430 mV	N/A	***Adv. Funct. Mater.***, 2015, 25, 393.
Co-P	0.1 mg cm^{-2}	300 mV	65	***Adv. Mater.***, 2015, DOI:10.1002/adma.201500894
CoOx@CN	0.12 mg cm^{-2}	380 mV	N/A	***J. Am. Chem. Soc.***, 2015, 137, 2688.
$Ni_{0.33}Co_{0.67}S_2$ NWs	0.3 mg cm^{-2}	370 mV	60	***Adv. Energy Mater.***, 2015, 5, DOI:10.1002/aenm.201402031.
nNiFe-LDH/NGF	0.25 mg cm^{-2}	337 mV	45	***Adv. Mater.,*** 2015, DOI:10.1002/adma.201501901
NiCo-r	0.28 mg cm^{-2}	320 mV	30	***Angew. Chem. Int. Ed.***, 2015, DOI: 10.1002/anie.201502226.
NiFe-LDH-CNTs	0.25 mg cm^{-2}	250 mV	31	***J. Am. Chem. Soc.***, 2013, 135, 8452.
α-$Ni(OH)_2$ spheres	0.2mg cm^{-2}	331 mV	42	***J. Am. Chem. Soc.***, 2014, 136, 7077.
$CoSe_2$ nanosheet	0.14 mg cm^{-2}	330 mV	44	***J. Am. Chem. Soc.***, 2014, 136, 15670.
CoMn LDH	0.14 mg cm^{-2}	320 mV	43	***J. Am. Chem. Soc.***, 2014, 136, 16481.
NiCo binary oxide	N/A	325 mV	39	***ACS Nano***, 2014, 8, 9518–9523.
NG-CNT	N/A	520 mV	141	***Adv. Mater.***, 2014, 26, 2925.

Table S3. Comparison of our $Ni_{0.9}Fe_{0.1}$/NC catalyst with some recently reported nonprecious HER electrocatalysts in alkaline media measured on **glassy carbon electrode**.

Catalyst	Mass loading	Overpotential vs. RHE for j=10 mA cm^{-2}	Tafel slope mV/dec	Reference
$Ni_{0.9}Fe_{0.1}$/NC	0.2 mg cm^{-2}	231 mV	111	*This work.*
Co-NRCNTs	0.28 mg cm^{-2}	370 mV	N/A	***Angew. Chem. Int. Ed.,*** 2014, 53, 4372.
Ni/MWCNT	N/A	350 mV	139	***J. Power Sources,*** 2014, 266, 365
CoP/CC	0.92 mg cm^{-2}	209 mV	129	***J. Am. Chem. Soc.***, 2014, 136, 7587.
MnNi/C	0.28 mg cm^{-2}	360 mV	N/A	***Adv. Funct. Mater.***, 2015, 25, 393.
CoOx@CN	0.12 mg cm^{-2}	230 mV	N/A	***J. Am. Chem. Soc.***, 2015, 137, 2688.
MoB	2.5 mg cm^{-2}	225 mV	59	***Angew. Chem. Int. Ed.***, **2012**, 51, 12703
MoP	0.86 mg cm^{-2}	130 mV	48	***Energy Environ. Sci.***, 2014, 7, 2624.
Ni/NiO-CNT	0.28 mg cm^{-2}	100 mV	N/A	***Nat. Commun.***, 2014, 5,4695
MoC_x	0.86 mg cm^{-2}	180 mV	59	***Nat. Commun.***, 2015, 6, 6512.
np-CuTi	N/A	50 mV	110	***Nat. Commun.***, 2015, 6, 6567.
Ni/N/C	0.4 mg cm^{-2}	200 mV	N/A	***Adv. Energy Mater.,*** 2015, 5, DOI:10.1002/aenm.201401660

Table S4. Comparison of our $Ni_{0.9}Fe_{0.1}$/NC catalyst with some recently reported nonprecious bifuntional electrocatalysts for **two-electrode water splitting cell** in alkaline media.

Catalyst	Catalyst support	Mass loading	Overall voltage for j=10 mA cm^{-2}	Reference
$Ni_{0.9}Fe_{0.1}$/NC	Ni foam	2.0 mg cm^{-2}	1.58 V	*This work.*
$Ni_{0.9}Fe_{0.1}$/NC	CFPs	2.0 mg cm^{-2}	1.64 V	*This work.*
NiFe LDH	Ni foam	Unknown	1.7 V	***Science***, 2014, 345, 1593.
Ni_5P_4	Ni foam	3.5 mg cm^{-2}	1.7 V	***Angew. Chem. Int. Ed.***, 2015, 54, DOI: 10.1002/anie.201502438.
Co-P	Cu foil	Unknown	1.65 V	***Angew. Chem. Int. Ed.***, 2015, 54, 6251.
$Ni_{0.33}Co_{0.67}S_2$ NWs	Ti foil	0.3 mg cm^{-2}	1.72 V	***Adv. Energy Mater.***, 2015, 5, DOI:10.1002/aenm.201402031..
NiSe NWs	Ni foam	3.5 mg cm^{-2}	1.63 V	***Angew. Chem. Int. Ed.***, 2015, 54, DOI: 10.1002/anie.201503407.
CoOx@CN	Ni foam	2 mg cm^{-2}	1.68 V	***J. Am. Chem. Soc.***, 2015, 137, 2688.
Ni_2P NPs	Ni foam	5 mg cm^{-2}	1.63 V	***Energy Environ. Sci.***, 2015, **8**, 2347.
Li-NiFeOx	CFPs	3 mg cm^{-2}	1.51 V	***Nat. Commun.***, 2015, 6, 7261.

Additional References

(1) Gong, M.; Zhou, W.; Tsai, M.-C.; Zhou, J.; Guan, M.; Lin, M.-C.; Zhang, B.; Hu, Y.; Wang, D.-Y.; Yang, J.; Pennycook, S. J.; Hwang, B.-J.; Dai, H. *Nat. Commun.* **2014**, 5, 4695.

(2) Gong, M.; Li, Y.; Wang, H.; Liang, Y.; Wu, J. Z.; Zhou, J.; Wang, J.; Regier, T.; Wei, F.; Dai, H. *J. Am. Chem. Soc.* **2013,** 135, 8452-8455.